Tunable Impedance-Matching Filters

José Antonio Estrada, *Member, IEEE*, Seth Johannes, *Member, IEEE*,
Dimitra Psychogiou, *Senior Member, IEEE*, and Zoya Popović, *Fellow, IEEE*

***Abstract*— In this letter, we present a general design method for tunable matching networks that have a prescribed filter characteristic over a range of complex port impedances. The approach enables prediction of the achievable tunable impedance range, given a filter topology and tuning element values. As experimental validation, a 2.5-GHz second-order Chebyshev filter is designed using Skyworks SMV2205-040LF varactor diodes to tune the filter resonator and inverter. It is shown that the filter can match port impedances in a region that spans a range of real and imaginary parts of the impedance between 10 and 150 Ω with an insertion loss of 1.5 dB.**

***Index Terms*— Coupling matrix, filter, impedance tuning.**

I. Introduction

IN MICROWAVE front ends, filtering is required between cascaded components, e.g., a power amplifier (PA) and antenna in a transmitter as shown in Fig. 1. The antenna impedance can vary due to scanning in a phased array (e.g., [1]) or changing surroundings as in a hand-held device (e.g., [2], [3]). The active device of a PA generally requires a complex impedance match for best power, gain, or efficiency and this can vary over output power and supply voltage in applications such as envelope tracking (e.g., [4]). In dynamic load-modulation of PAs one also requires tunable load impedances [5]. Various other applications such as microwave cooking, plasma generation [6], RF tumor ablation [7], and beamforming MIMO [8] present loads that vary in time and require adaptability. Such impedance variations can be compensated with tuning networks, which are typically lossy, e.g., [2], [9], or have limited power handling capabilities, e.g., [8], [10], [11]. Filters designed as real-to-real impedance transformers are discussed in, e.g., [12], [13], and a filter the frequency of which tunes to a complex antenna is shown in [14]. In [15] the antenna is integrated with the filter achieving frequency tuneability, and in [16] an amplifier is integrated with a frequency-tunable filter.

The goal of this work is to develop a design procedure and demonstrate an impedance-tuning network with a specific filter spectral response in order to reduce the footprint and loss of the front end. The fixed network design approach in [17] is extended to a tunable network design. We demonstrate the approach on a 2.5-GHz second-order Chebyshev filter with one fixed 50-Ω port, while the impedance on the other port can be tuned over a range of real and imaginary parts of the impedance between 15 and 150 Ω.

Manuscript received February 28, 2021; revised April 29, 2021; accepted May 1, 2021. Date of publication May 24, 2021; date of current version August 9, 2021. This work was supported in part by the NSF SpeCEESprogram under Grant ECCS-1731956. *(Corresponding author: José Antonio Estrada.)*

The authors are with the Department of Electrical, Computer, and Energy Engineering, University of Colorado at Boulder, Boulder, CO 80309 USA (e-mail: jose.estrada@colorado.edu).

Color versions of one or more figures in this letter are available at https://doi.org/10.1109/LMWC.2021.3083184.
Digital Object Identifier 10.1109/LMWC.2021.3083184

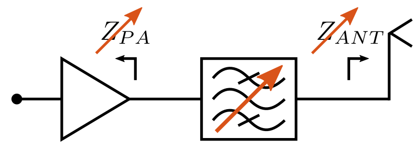

Fig. 1. Transmitter front end, where both antenna impedance and PA output impedance can vary and can be matched with the tunable filter.

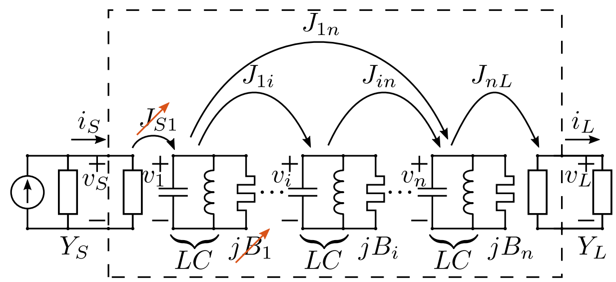

Fig. 2. Filter diagram for an impedance tunable second-order all-pole filter, showing the two necessary tunable elements.

II. Design Methodology

The port impedance of a coupled resonator filter can be modified by adjusting the resonant frequency and the coupling to the first resonator [17]. This impedance modification does not alter the frequency response of the filter as long as it remains conjugately matched on both ports as shown in the appendix of [17]. Fig. 2 shows the diagram of a filter with a tunable port impedance, showing the tunable elements.

The first admittance inverter value is given by Hong [18] and Cameron *et al.* [19]

$$J_{S1} = m_{S1}\sqrt{\frac{2\pi f_0 C\Delta}{R_S}} \tag{1}$$

where m_{S1} is the coupling matrix element for the source to resonator 1 coupling, f_0 is the center frequency, Δ is the fractional bandwidth, C is the base resonator capacitance and R_S is the reference port resistance, which in our case is the real part of the target complex impedance $Z_S = R_S + jX_S$, which is the complex conjugate of the impedance the filter will present at its poles. The resonant frequency of the first resonator can be derived as

$$f_{01} = f_0\left[\sqrt{1+\left(\frac{m_{11}\Delta}{2}\right)^2} - \frac{m_{11}\Delta}{2}\right] \tag{2}$$

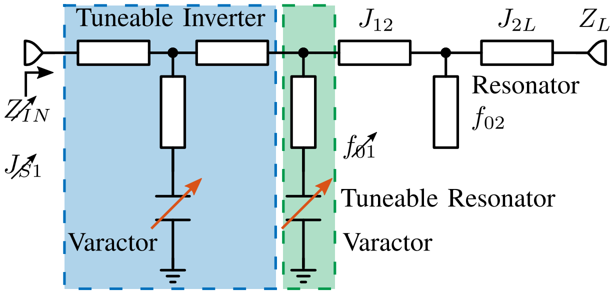

Fig. 3. Schematic of the second-order filter. The shaded areas are the tunable input inverter (blue) and the tunable resonator (green).

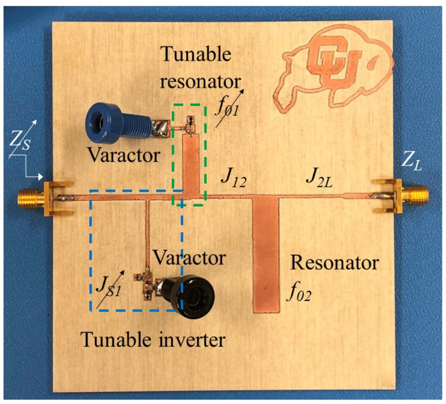

Fig. 4. Photograph of the 2.5-GHz filter, where the blue and green shaded rectangles areas correspond to those in Fig. 3.

where $m_{11} = m_{110} + \Delta m_1$ is the coupling matrix element for the first resonator. This element can be used to adjust the imaginary part of the port impedance by Estrada *et al.* [17]

$$\Delta m_1 = -x_S m_{S1}^2 = -\frac{X_S}{R_S} m_{S1}^2 \tag{3}$$

where m_{110} is the original coupling matrix element of a filter terminated in a real impedance.

The source to resonator 1 coupling (m_{S1}) modifies both the real and imaginary parts. The resonant frequency can be controlled by using a capacitively terminated stub with a variable capacitance and provides control over the imaginary part of the impedance. A tunable inverter can be approximated using transmission line inverters [18] with a similar tunable stub. Both circuit elements can be controlled using varactor diodes, as illustrated in Fig. 3.

The input impedance of the filter is given by

$$Z_{\text{in}} = Z_S^* = \left(\frac{C\omega_0\Delta}{J_{S1}^2}\right)\left[1 + j\frac{1}{\Delta}\left(\frac{f_0}{f_{01}} - \frac{f_{01}}{f_0}\right)\right] \tag{4}$$

where $\omega_0 = 2\pi f_0$. In this equation, it can be explicitly seen that the real and imaginary parts can be controlled by modifying J_{S1} and that changing f_{01} modifies the imaginary part exclusively.

A demonstrator filter with the schematic shown in Fig. 3 is implemented in microstrip. The input inverter (J_{S1}) and the first resonator (f_{01}) are implemented with varactor-loaded stubs, while the other two inverters (J_{12} and J_{2L}) are implemented with quarter-wavelength lines and the second resonator

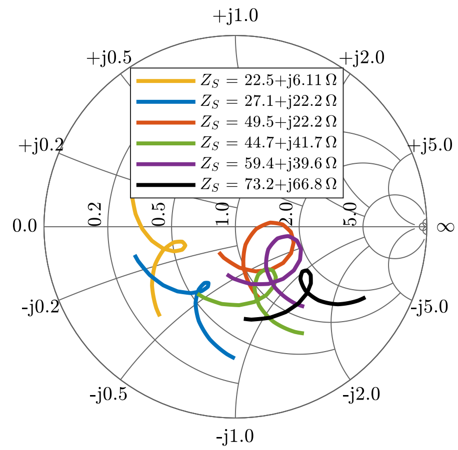

(a)

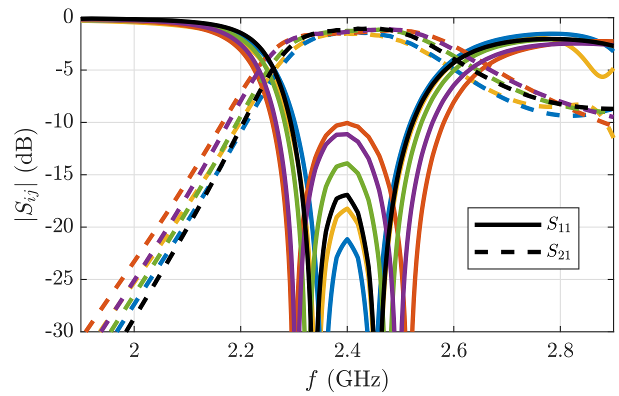

(b)

Fig. 5. Simulated filter performance. (a) Input reflection coefficient from 2.26 to 2.54 GHz on a 50-Ω Smith chart for different varactor bias voltages. (b) Frequency response for the different filter configurations. As the impedance deviates from the nominal $Z_S = (45 - j42)$ Ω, the quality of the match and the bandwidth present small variations, as expected.

(f_{02}) is a half-wavelength open stub resonator. A varactor is used to tune the resonator, and an anti-series varactor connection is used for inverter tuning. The impedance tuning range is limited by the tunable inverter J_{S1}, which increasingly differs from an ideal inverter as the capacitance of the varactor varies farther from the central design value.

III. Filter Design

The filter is designed to be an in-line all-pole filter with 15-dB return loss. The coupling matrix for that filter is

$$[m] = \begin{bmatrix} 0 & 1.0369 & 0 & 0 \\ 1.0369 & 0 & 1.2868 & 0 \\ 0 & 1.2868 & 0 & 1.0369 \\ 0 & 0 & 1.0369 & 0 \end{bmatrix}. \tag{5}$$

The filter response is centered at 2.4 GHz with 9% bandwidth. The port impedance of the filter is designed to cover a region in the lower (capacitive) half of the Smith chart, "centered" around a nominal impedance of $(45 - j42)\Omega$. Simulations are performed in Cadence AWR, the circuit is EM simulated using Axiem, the diodes, and discrete passive (packaged) components are simulated using Modelithics models. The resulting layout is seen in Fig. 4 where the differ-

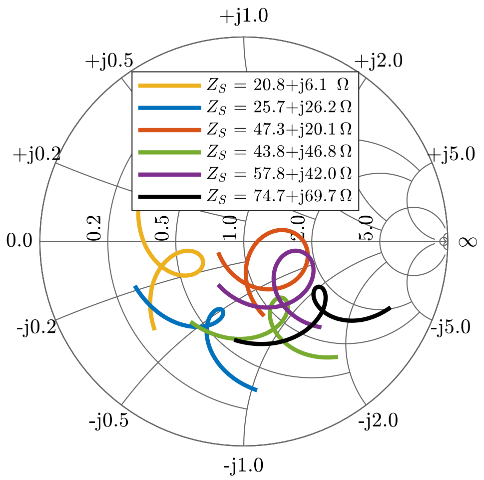

(a)

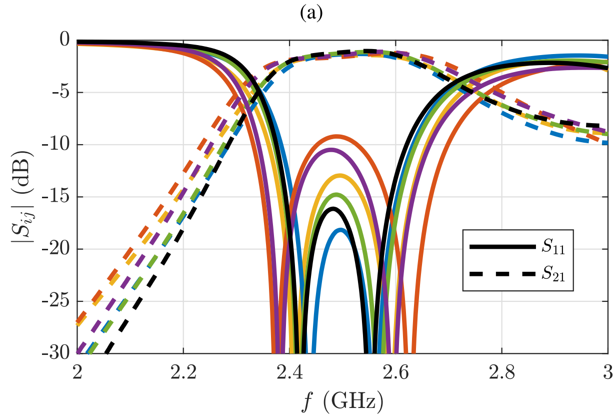

(b)

Fig. 6. Measured filter performance. (a) Input reflection coefficient, from 2.35 to 2.65 GHz, on a 50-Ω Smith chart for different configurations. (b) Frequency response for those different filter configurations. The green lines correspond to the center of the varactor bias range.

ent components of the circuit are labeled in correspondence to Fig. 3.

The microstrip filter uses a Rogers RO4350B substrate with 762-μm dielectric thickness and 35-μm copper thickness. The variable capacitors are SMV2205-040LF varactor diodes from Skyworks which use a continuous control voltage from 2 to 10 V. The capacitance values for the design are closer to those of a single varactor for the resonator (3–15 pF) and an anti-series configuration for the inverter capacitance (1.5–7.5 pF). If the tuner is used at the output of a PA, the reverse breakdown and reduced capacitance range at higher powers become important factors. Since it is difficult to find commercial varactors with high reverse breakdown voltages, the anti-series diode combination is a possible option, as in [20]. The bias lines are implemented with lumped-element inductors and capacitors.

The simulated performance of the filter in 5. Fig. 5(a) shows the port complex impedance around the passband. The loops cross at the filter poles which are located at each side of the center frequency of the filter and occur when the impedance looking into the filter is the complex conjugate of the port impedance (Z_S). Fig. 5(b) shows the frequency response which maintains shape for the different varactor voltages. The loop size on the Smith chart is related to the match at the center frequency and the bandwidth. For the larger loops, where the impedance is the farthest from the loop crossing, the return loss is worse. The bandwidth and insertion loss of the filter do not vary considerably. Note that the center biasing for the varactors corresponds to the center impedance within the range (shown by the green line in the figures).

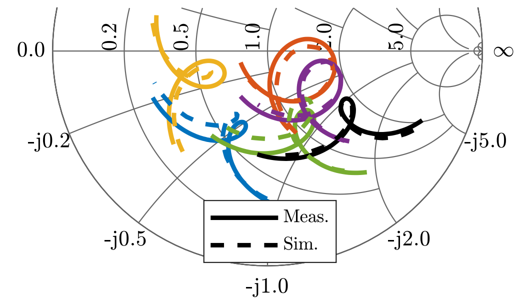

Fig. 7. Measured and simulated comparison of filter input reflection coefficient around the center of the band. The colors correspond to the values of Z_S from Figs. 5 and 6.

IV. Measurement Results

The fabricated filter is shown in the inset of Fig. 3. Additional 50-Ω transmission line segments are added at the input and output, and a TRL calibration is performed with reference planes exactly at the filter, which is critical when measuring a circuit with a non-standard port impedance. The measured performance is shown in Fig. 6 where it can be seen that the filter center frequency is shifted by 4%. The return loss remains larger than 10 dB in the passband with a large portion of the Smith chart covered. The insertion loss for the worst case is 1.5 dB and can be improved with higher Q-factor resonators. Simulations were repeated with lossless elements at several frequencies and the additional loss due to the transmission lines is determined to be 0.55 dB. If diodes with a larger capacitance range are used, the overall impedance range would increase, but not linearly due to diminishing returns resulting from changes in the filter function shape. Fig. 7 shows the comparison of simulation and measurement.

V. Conclusion

We present a second-order Chebyshev filter with a tunable input impedance with a maintained filter response. The demonstrator filter uses varactor diodes, but the proposed technique can be extended to tuning with piezoelectric elements [21], MEMS [22], [23], liquid metal [24], and PIN diodes [25]. The impedance tunability can be extended to the other port in a straightforward manner. The method shown here is valid for a relatively narrow bandwidth, and scaling to larger bandwidths and impedance ranges is under investigation.

Acknowledgment

Seth Johannes and Zoya Popović acknowledge support through the Lockheed Martin Endowed Chair of RF Engineering; and José Antonio Estrada is grateful for the Summer Graduate Fellowship at the University of Colorado at Boulder, Boulder, CO, USA.

REFERENCES

[1] R. W. Kindt and J. T. Logan, “Benchmarking ultrawideband phased antenna arrays: Striving for clearer and more informative reporting practices,” *IEEE Antennas Propag. Mag.*, vol. 60, no. 3, pp. 34–47, Jun. 2018.

[2] L. Sankey and Z. Popovic, “Adaptive tuning for handheld transmitters,” in *IEEE MTT-S Int. Microw. Symp. Dig.*, Jun. 2009, pp. 225–228.

[3] K. R. Boyle, Y. Yuan, and L. P. Ligthart, “Analysis of mobile phone antenna impedance variations with user proximity,” *IEEE Trans. Antennas Propag.*, vol. 55, no. 2, pp. 364–372, Feb. 2007.

[4] S. Schafer and Z. Popović, “Multi-frequency measurements for supply modulated transmitters,” *IEEE Trans. Microw. Theory Techn.*, vol. 63, no. 9, pp. 2931–2941, Sep. 2015.

[5] W. Hallberg, D. Gustafsson, M. Ozen, C. M. Andersson, D. Kuylenstierna, and C. Fager, “A class-J power amplifier with varactor-based dynamic load modulation across a large bandwidth,” in *IEEE MTT-S Int. Microw. Symp. Dig.*, May 2015, pp. 1–4.

[6] A. Al Bastami *et al.*, “Dynamic matching system for radio-frequency plasma generation,” *IEEE Trans. Power Electron.*, vol. 33, no. 3, pp. 1940–1951, Mar. 2018.

[7] D. Haemmerich, “Mathematical modeling of impedance controlled radiofrequency tumor ablation and *ex-vivo* validation,” in *Proc. Annu. Int. Conf. IEEE Eng. Med. Biol.*, Aug. 2010, pp. 1605–1608.

[8] I. Vasilev, J. Lindstrand, V. Plicanic, H. Sjöland, and B. K. Lau, “Experimental investigation of adaptive impedance matching for a MIMO terminal with CMOS-SOI tuners,” *IEEE Trans. Microw. Theory Techn.*, vol. 64, no. 5, pp. 1622–1633, May 2016.

[9] A. Semnani, G. S. Shaffer, M. D. Sinanis, and D. Peroulis, “High-power impedance tuner utilising substrate-integrated evanescent-mode cavity technology and external linear actuators,” *IET Microw., Antennas Propag.*, vol. 13, no. 12, pp. 2067–2072, Oct. 2019.

[10] T. Vaha-Heikkila, J. Varis, J. Tuovinen, and G. M. Rebeiz, “A 20-50 GHz RF MEMS single-stub impedance tuner,” *IEEE Microw. Wireless Compon. Lett.*, vol. 15, no. 4, pp. 205–207, Apr. 2005.

[11] D. Qiao *et al.*, “Antenna impedance mismatch measurement and correction for adaptive CDMA transceivers,” in *IEEE MTT-S Int. Microw. Symp. Dig.*, Jun. 2005, p. 4.

[12] R. Gomez-Garcia, D. Psychogiou, and D. Peroulis, “Reconfigurable single/multi-band planar impedance transformers with incorporated bandpass filtering functionality,” in *IEEE MTT-S Int. Microw. Symp. Dig.*, May 2016, pp. 1–4.

[13] R. Gómez-García, J. Muñoz-Ferreras, and D. Psychogiou, “Multi-band reflectionless filtering impedance transformers,” in *IEEE MTT-S Int. Microw. Symp. Dig.*, May 2018, pp. 1–4.

[14] T.-C. Lee, “Synthesis of microwave and acoustic wave resonator filters for wireless communication systems,” Ph.D. dissertation, School Elect. Comput. Eng., Purdue Univ., West Lafayette, IN, USA, 2014.

[15] R. E. Lovato, T. Li, and X. Gong, “Tunable filter/antenna integration with bandwidth control,” *IEEE Trans. Microw. Theory Techn.*, vol. 67, no. 10, pp. 4196–4205, Oct. 2019.

[16] K. Chen, T. Lee, and D. Peroulis, “Co-design of multi-band high-efficiency power amplifier and three-pole high-Q tunable filter,” *IEEE Microw. Wireless Compon. Lett.*, vol. 23, no. 12, pp. 647–649, Dec. 2013.

[17] J. A. Estrada, J. R. Montejo-Garai, P. de Paco, D. Psychogiou, and Z. Popović, “Power amplifiers with frequency-selective matching networks,” *IEEE Trans. Microw. Theory Techn.*, vol. 69, no. 1, pp. 697–708, Jan. 2021.

[18] J. Hong, *Microstrip Filters for RF/Microwave Applications* (Wiley Series in Microwave and Optical Engineering). Hoboken, NJ, USA: Wiley, 2011, ch. 7.

[19] R. Cameron, C. Kudsia, and R. Mansour, *Microwave Filters for Communication Systems*. Hoboken, NJ, USA: Wiley, 2018, ch. 8.

[20] A. S. Tehrani, H. M. Nemati, H. Cao, T. Eriksson, and C. Fager, “Dynamic load modulation of high power amplifiers with varactor-based matching networks,” in *IEEE MTT-S Int. Microw. Symp. Dig.*, Jun. 2009, pp. 1537–1540.

[21] E. J. Naglich, J. Lee, D. Peroulis, and W. J. Chappell, “Tunable, substrate integrated, high Q filter cascade for high isolation,” in *IEEE MTT-S Int. Microw. Symp. Dig.*, May 2010, pp. 1468–1471.

[22] M. A. El-Tanani and G. M. Rebeiz, “High-performance 1.5–2.5-GHz RF-MEMS tunable filters for wireless applications,” *IEEE Trans. Microw. Theory Techn.*, vol. 58, no. 6, pp. 1629–1637, Jun. 2010.

[23] X. Liu, L. P. B. Katehi, W. J. Chappell, and D. Peroulis, “High-Q tunable microwave cavity resonators and filters using SOI-based RF MEMS tuners,” *J. Microelectromech. Syst.*, vol. 19, no. 4, pp. 774–784, Aug. 2010.

[24] D. Psychogiou and K. Sadasivan, “Tunable coaxial cavity resonator-based filters using actuated liquid metal posts,” *IEEE Microw. Wireless Compon. Lett.*, vol. 29, no. 12, pp. 763–766, Dec. 2019.

[25] C. Lugo and J. Papapolymerou, “Electronic switchable bandpass filter using PIN diodes for wireless low cost system-on-a-package applications,” *IEE Proc., Microw., Antennas Propag.*, vol. 151, no. 6, pp. 497–502, Dec. 2004.